Phase states of dynamically compressed cerium

V. M. Elkin, V. N. Mikhaylov, and A. V. Petrovtsev

Russian Federal Nuclear Center - Zababakhin Institute of Applied Physics, Snezhinsk, Russia

F. J. Cherne

Los Alamos National Laboratory, Los Alamos, New Mexico, USA

This paper presents a multiphase equation of state for cerium, which includes the γ, α, ε, and liquid phases. The α and γ phases are described with the Aptekar-Ponyatovsky model for pseudobinary solutions, while the ε and liquid phases are treated as pure phases. The Hugoniot and release isentropes are calculated for the solid γ, α, liquid, and mixed phases. Based on the model developed, the Hugoniot does not cross the line of the α-ε transition and melting occurs directly from the α phase. The equation of state developed shows reasonable agreement with the static measurements, the experimentally determined phase diagram, and the shock experimental data. Cerium compresses isentropically through the γ-α transition as a result of cerium's abnormal compressibility in the region of the γ-α transition. The inclusion of the Aptekar-Ponyatovsky model assists in providing a way to handle both the abnormal compressibility and the anomalous melt boundary simultaneously. Experimentally under dynamic loading conditions, a three-wave structure is observed at stresses above the phase transition: an elastic wave, a phase transition wave (which appears as an isentropic compression wave), followed by a shock wave. For our model development we consider only the hydrostatic response and thus a two-wave structure would be anticipated. No phase precursor would be observed for melting. Sound velocity behind the shock front dramatically decreases in the region of the γ-α transition and smoothly varies through the region of melting.

I. INTRODUCTION

Accurate simulation of the propagation of compression waves hinges upon the underlying equation of state for the material of interest. As one simulates phase-transforming materials one can gain insights into the underlying processes that may be taking place. The development of multiphase semiempirical equations of state has been with us for the last 30 years. Early works on iron[1] and bismuth[2,3] laid the foundation for later works on other phase-transforming materials.[4–8] This work follows these works by developing an equation of state for cerium.

There are many allotropic phase regions present in the phase diagram in cerium; here we present a multiphase equation of state covering four of cerium's phases, namely, α, γ, ε, and liquid. Cerium has a number of unusual properties, the most important of which are the solid-solid critical point on the line of the isomorphic γ-α transition and the abnormal behavior of its elastic and thermal properties in the neighborhood of the γ-α transition. The reason for this unusual behavior is likely due to $4f$ electrons whose role in chemical bonding changes in response to ambient conditions. In this context, there is a great amount of interest in studying this material's dynamic response when undergoing shock compression. In prior papers,[9,10] we presented equation of state parameters for the α and γ phases of cerium based on the Aptekar-Ponyatovsky (AP) model for pseudobinary solid solutions.[11,12] The AP model treats cerium as a solid substitution solution consisting of cerium atoms in different electronic states. Unlike the typical two-component systems, the proportion of atoms at different electronic states is not fixed, yet is defined by a minimum in the thermodynamic potential which is dependent upon temperature and pressure. The AP model adequately describes cerium anomalies in the region of the isomorphic γ-α transition, including the solid-solid critical point. On account of its abnormal compressibility

$[(\partial^2 V/\partial P^2)_S < 0]$, cerium compresses isentropically through the γ-α transition. Increasing the magnitude of dynamic compression beyond the phase transition stress leads to an observed two-wave configuration: a phase precursor (the isentropic compression wave) followed by a shock wave. As shock strength increases, the apparent transition stress from the phase precursor decreases continuously and the two-wave configuration disappears, at which point the phase precursor is totally overdriven. These features have been experimentally verified by Borisenok *et al.*[13]

For this work we include additional phases for cerium into the equation of state, namely, the liquid (*L*) phase and the ε phase. The phase stability region for each of the phases is presented as well as the shock compression behavior well into the melt.[9,10] As in prior papers, the equation of state for the α and γ phases is based on the AP model. A slight modification of the α and γ was made to improve the fits. The liquid and ε phases are considered as individual (pure) phases. The phases we do not consider are the β phase (DHCP—a small region in the phase diagram obtained by multiple thermocycling around room temperature), the high-temperature δ phase (which is bounded by the γ phase and the melt boundary for pressures less than $\sim$2.6 GPa), and the α' and α'' phases having the orthorhombic (α-*U*) and monoclinic structures.

In Sec. II we give the essentials of the AP model and EOS models for individual phases. Section III compares calculated and experimental static thermodynamic properties. Finally, Sec. IV discusses the dynamic experimental data, as well as discussing potential implications arising from the equation of state.

II. BASIC EQUATION-OF-STATE RELATIONS

For each of the individual phases (α, γ, ε, and liquid) a Helmholtz free-energy function is developed. The basic

formalism for the Helmholtz energy is given as a sum of four components:

$$F(V,T) = F_C(V) + F_H(V,T) + F_{AE}(V,T) - S_{tr}T, \qquad (1)$$

where F_C is the cold energy, F_H is the quasiharmonic free energy, F_{AE} is the anharmonic-electronic free energy associated with phonon-phonon interactions and thermally excited electron energies, and $S_{tr}T$ is an entropy of transition term. The entropy contribution term is used to account for the disordering entropy in melting and contributions from the crystal field, spin fluctuations, etc., as well as the entropy associated with the isomorphic $(\alpha$-$\gamma)$ transition. As shown by Jeong *et al.,*[14] the change in vibrational entropy which is accounted for, in the quasiharmonic free energy term only contributes to about half the total entropy change that occurs during the α-γ transition. We acknowledge that treating the liquid phase as a quasiharmonic solid is a simplification, yet it has been shown by Chisolm[15] and Wallace[16] to be appropriate, assuming some degree of short-range ordering exists in the liquid. Therefore we include a constant value of S_{tr} in the γ and the liquid phases which only influences the melt boundary and the α-γ phase boundary. At low temperatures the α phase is the energetically preferred phase and thus the constant S_{tr} does not play a role in the entropy of cerium. In Eq. (1) the quasiharmonic and the anharmonic-electronic free energies contribute to the thermal dependence of the total entropy of the phase.

The cold energy, $F_C \equiv E_C(V)$, describes the atomic interaction energy in a static lattice at $T = 0$ K. It is determined by integrating an expression for pressure (a modified universal EOS by Vinet *et al.*[17]) by volume. The expression for the pressure as a function of volume is given by

$$P_C(y) = 3B_{0K} \frac{1-y}{y^2} \exp[\eta(1-y) + \beta(1-y)^2], \qquad (2)$$

where $y = (V/V_{0K})^{1/3}$. V_{0K} and B_{0K} are the specific volume and bulk modulus, respectively, at $P = 0$ and $T = 0$ K. The parameters η and β relate to the first (B'_{0K}) and second (B''_{0K}) pressure derivatives of the bulk modulus (at $y = 1$): $B'_{0K} = (2\eta + 3)/3$, $B''_{0K} = -[\eta^2 + \eta - 6\beta + 2]/(9B_{0K})$.

The second term in the sum, the quasiharmonic free energy F_H, is described by the Debye approximation:

$$F_H = RT\left[\frac{9}{8}\tau + 3\ln(1 - e^{-\tau}) - D(\tau)\right], \qquad (3)$$

where $\tau \equiv \theta_D(V)/T$. $\theta_D(V) = \theta_{D0}\exp(-\int_{V_{0K}}^{V} \frac{\Gamma_H(t)}{t}dt)$ is the Debye temperature, and $D(y) = \frac{3}{y^3}\int_0^y \frac{t^3}{e^t - 1}dt$ is the Debye function. The Gruneisen function $\Gamma_H(V)$ is assumed to be equal to an adjustable constant Γ_0, which is determined from the fitting procedure.

The contribution to the Helmoltz free energy attributed to anharmonic lattice oscillations and thermally excited electrons is given by the following function: $F_{AE} = -\frac{1}{2}Dx^{\Gamma_{AE}}T^2$, where D and Γ_{AE} are free (adjustable) parameters.

For the γ-α phase region the AP model is applied in a similar fashion as in Refs. 9 and 10. The AP model constructs a thermodynamic Gibbs potential which describes the region as a thermodynamic coexistence of atoms in the different electronic states corresponding to either the α or the γ phases. The Gibbs potential is written as

$$\begin{aligned} G = {}&(1 - c)G_{\alpha_0} + cG_{\gamma_0} + c(1 - c)G_{\text{mix}} \\ &+ TR[c\ln c + (1 - c)\ln(1 - c)], \end{aligned} \qquad (4)$$

where T is temperature, G_{α_0} and G_{γ_0} are the thermodynamic Gibbs potentials of the individual (pure) phases α_0 and γ_0, respectively, c is the concentration of atoms whose electron configuration corresponds to the γ_0 phase, G_{mix} is a mixing potential, and R is the universal gas constant. The Gibbs potentials, $G(V,T)$, are determined from the relations $G = F + PV$, where volume V is determined from the solution to

$$P = \left(\frac{\partial F}{\partial V}\right)_T. \qquad (5)$$

At specified P and T, the equilibrium concentration c is determined from obtaining the minimum of the thermodynamic potential:

$$\begin{aligned} \left(\frac{\partial G}{\partial c}\right)_{P,T} &= 0, \\ \left(\frac{\partial^2 G}{\partial c^2}\right)_{P,T} &> 0. \end{aligned} \qquad (6)$$

When $c > 0.5$ the solid solution is said to be in the γ phase, and similarly when $c < 0.5$ the phase state is said to be in the α phase. At the limiting values of c, the pure (individual) phases are obtained γ_0 ($c = 1$) and α_0 ($c = 0$). The minimum of the potential given by Eq. (6) has one or two solutions (depending on particular values of the variables contained therein). Please see the Appendix for more details. The thermodynamic potential's minima correspond to concentrations c_1 and c_2, which may have identical or different depths depending on the magnitudes of G_{γ_0} and G_{α_0}. Physically, the existence of different depth minima provides for metastability for the phase with greater Gibbs free energy. When the Gibbs energies are identical [i.e., $G(P,T,c_1) = G(P,T,c_2)$], phase equilibrium is reached. It can be shown[11] that in this case $c_1 = 1 - c_2$ and $G_{\alpha_0} - G_{\gamma_0} = 0$. Thus, the phase equilibrium line for the α and γ phases of the pseudobinary solution coincides with the phase equilibrium line for the pure α_0 and γ_0 phases. Near the phase equilibrium line, one phase is metastable (i.e., higher Gibbs free energy phase) and one phase is stable (i.e., lower Gibbs free energy phase). Still further departure from the equilibrium line causes the metastable phase to lose its stability altogether; in other words, one solution to Eq. (6) exists.

At the conditions $(\frac{\partial G}{\partial c})_{P,T} = 0$ and $(\frac{\partial^2 G}{\partial c^2})_{P,T} = 0$ one of the minima vanishes on the (P,T) plane and the number of solutions for Eq. (6) changes to one possible solution. The critical point occurs where the two minima become one at $c_1 = c_2 = 1/2$ and the equality $(\frac{\partial^2 G}{\partial c^2})_{P,T} = 0$ is satisfied. The critical temperature can be determined from the equality $2RT_{cr} = G_{\text{mix}}(P,T_{cr})$. Using the same empirical form as was presented in Refs. 9 and 10, G_{mix} is defined as

$$G_{\text{mix}}(T) = G_{\text{mix}}^0\left[1 + \frac{\theta_1}{T} + \left(\frac{\theta_2}{T}\right)^2\right], \qquad (7)$$

where G_{mix}^0, θ_1, and θ_2 are adjustable parameters. The parameters G_{mix}^0, θ_1, and θ_2 were determined from the equality

$G_{mix}(T_{cr}) = 2RT_{cr}$ in the critical point, which was assumed to be $T_{cr} = 482.5$ K.[18,19] This functional representation for the mixing potential is a simplified version which was presented by Dzhavadov.[20] In the limit, as temperature approaches zero, it is clear that this functional representation fails because the function $G_{mix}(T)$ will tend toward infinity. However, at $T > 300$ K, this empirical form describes experimental data quite well. Unfortunately, there are still no physics-based models for the mixing potential. *Ab initio* simulations designed to consider the mixed states of cerium may assist in defining the physical processes around the α-γ phase boundary leading to a more appropriate semiempirical function for the G_{mix} term in Eq. (4).

Once again for clarity, we emphasize that the α and γ phases are understood to be different states of the solid solution (mixture) of the pure (individual) α_0 and γ_0 phases. The γ phase occurs in the region above the γ-α equilibrium curve with an extension beyond the critical point in temperature up to the melt boundary minimum, and for pressures below γ-α equilibrium curve with the extension beyond the critical point. The α phase occurs at temperatures below and pressures above the γ-α equilibrium curve and the extrapolation of the line beyond the critical point.

The challenge selecting parameters for multiphase equations of state arises because each phase must be coupled to the other phases. In other words, the parameters selected must be related to the phase diagram and the variations of various thermodynamic variables around the phase boundaries. A genetic algorithm (GA) method[21,22] simulates the natural evolutionary processes which was applied[23] to the optimization EOS parameters. The GA demonstrated high efficiency in obtaining parameters. An effectiveness function composed of a sum of weighted (based on confidence level in the data) dimensionless and normalized root-mean-square deviations between calculated and experimental data was developed. Tables I and II provide the parameters obtained for equations of state for the pure (individual) phases of cerium and for the α-γ mixing potential [Eq. (7)].

When selecting the EOS parameters for the α and γ phases only static data and phase boundary data were used. Shock experimental data are strongly scattered in this region and, thus, were not included in the EOS parameter fit. The

TABLE I. Parameters for the equations of state for the individual phases of cerium.

Parameter	Phase			
	α_0	γ_0	ε	Liquid
ρ_{0K} (g/cm^3)	8.352	6.789	8.526	7.757
B_{0K} (GPa)	24.841	22.609	26.862	24.688
B'_{0K}	3.70	3.40	6.636	4.625
β	60.3	0	0	11.3
θ_{D0} (K)	138.0	104.0	127.6	104
Γ_0	1.652	0.470	1.673	1.569
Γ_{AE}	0.93	1.79	1.70	1.18
D/R (10^{-3} 1/K)	2.12	0.73	0.21	0.64
E_{0K}/R (K)	0	273.2	161.3	3288.0
S_{tr}/R	0	1.30	0	4.19

TABLE II. Mixing potential parameters.

G_{mix}^0/R (K)	θ_1 (K)	θ_2 (K)
1288.9	−130.0	65.0

Debye temperature of the γ_0 phase was chosen based on its experimental value of 104 K.[14] For the liquid phase, the same Debye temperature was chosen, partly because at high temperatures this parameter only influences the entropy of melting. The parameter S_{tr} for the liquid phase was optimized to obtain the desired entropy of melting. The liquid phase EOS parameters were fitted to shock compression, liquid melt boundary, density, and thermal expansion data in the liquid phase of cerium. The calculated density, 6.88 g/cm^3, near the melting point and the calculated thermal expansion coefficient, 1.58×10^{-4} K^{-1}, for temperatures of 1100–1700 K agree well with the experimental values 6.87 ± 0.012 g/cm^3 and $(1.3 \pm 0.2) \times 10^{-4}$ K^{-1} obtained for the same conditions.[24] Parameters for the ε phases were selected from isothermal compression data[25] and the α-ε phase transformation curve.[26] An additional discussion on the selection of parameters for the ε phase will be discussed in the following section.

III. STATIC DATA COMPARED WITH EOS PREDICTIONS

Figures 1–8 compare calculated with experimental results for the following thermodynamic functions of the γ, α and ε phases: the pressure dependencies of bulk sound velocity[27] $C_B = (B_S/\rho)^{1/2}$ (B_S is the isentropic bulk modulus and ρ is density) and relative heat capacity $C_P(P)/C_P(0)$[28] (Fig. 1); isothermal compressibility χ versus pressure at different temperatures[29] (Fig. 2); the temperature dependencies of heat capacity C_P[30] and the coefficient of thermal expansion α_P[31] (Fig. 3); the thermal expansion coefficient versus temperature in the vicinity of the γ-α phase transformation at different pressures[29] (Fig. 4); the isentropic temperature variation with respect to pressure of cerium $(\partial T/\partial P)_S$ versus pressure at different temperatures[32] (Fig. 5) and versus temperature at different pressures (Fig. 6); the phase equilibrium line between
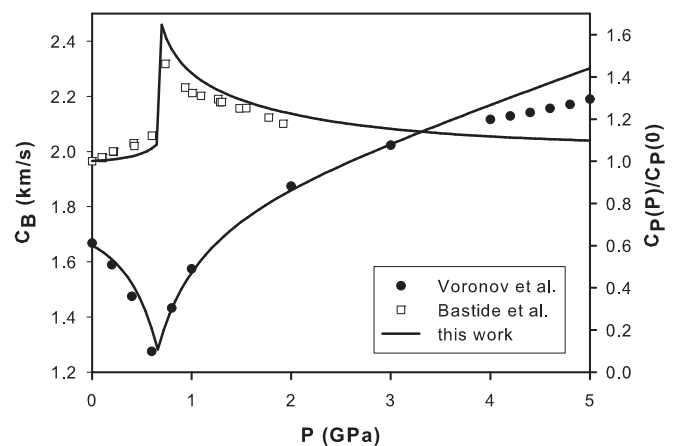

FIG. 1. Bulk sound velocity and relative heat capacity versus pressure at room temperature (experimental data from Refs. 27 and 28).
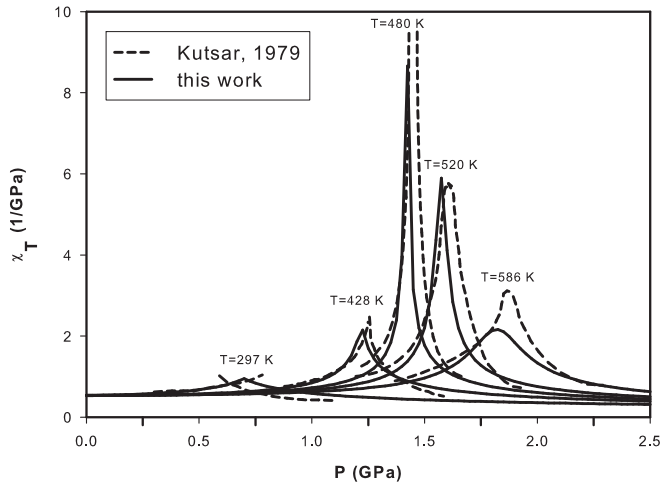
FIG. 2. Isothermal compressibility versus pressure at different temperatures (experimental data from Ref. 33).

FIG. 4. Thermal expansion coefficient versus temperature at different pressures (experimental data from Ref. 29).

the γ-α phases and the corresponding change in volume with respect to temperature on the phase equilibrium line, $\Delta V / V$ (Fig. 7);[33] and the molar volume V variation in isothermal compression[25,34,35] (Fig. 8). The resulting parameter set using the AP model shows that the calculated and experimental thermodynamic parameters of the γ and α phases are adequately capturing the abnormal response of cerium as a function of temperature and pressure.

In searching the literature for the thermophysical properties (thermal expansion and heat capacity) of the ε phase of cerium, it was determined that no data exist. This makes it difficult to determine appropriate parameters for the thermal components of the EOS. The parameters could be determined from the phase equilibrium lines between ε phase and other phases; however, information on the limits of ε phase stability is currently unreliable. Fig. 9 shows a phase diagram compiled from data presented by different authors.[26,33,36–39] Note that for this work the region indicated by the dashed line labeled T_{bell} (experimental data from[26,37,39]), the region of the α' and α'' phase stability, is not considered. The calculated line of γ-α

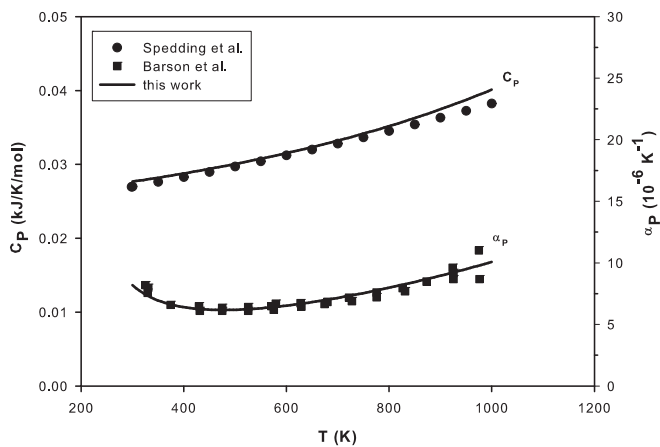FIG. 5. $\ln(\partial T / \partial P)_S$ versus pressure (experimental data from Ref. 32).

FIG. 3. Thermal expansion coefficient and heat capacity versus temperature at one atmosphere (experimental data from Refs. 30 and 31).
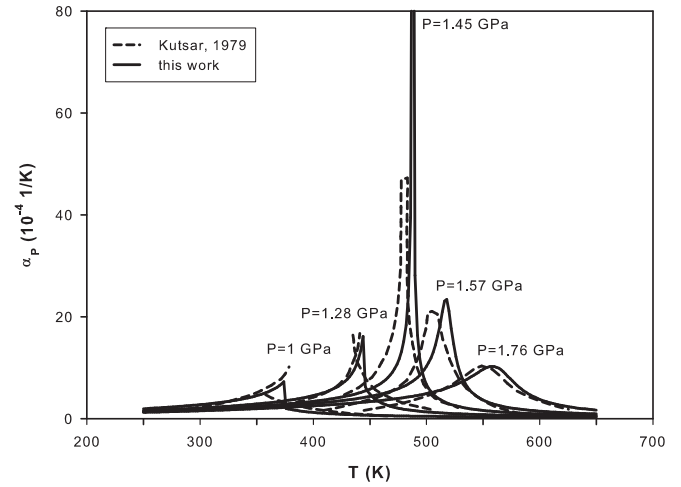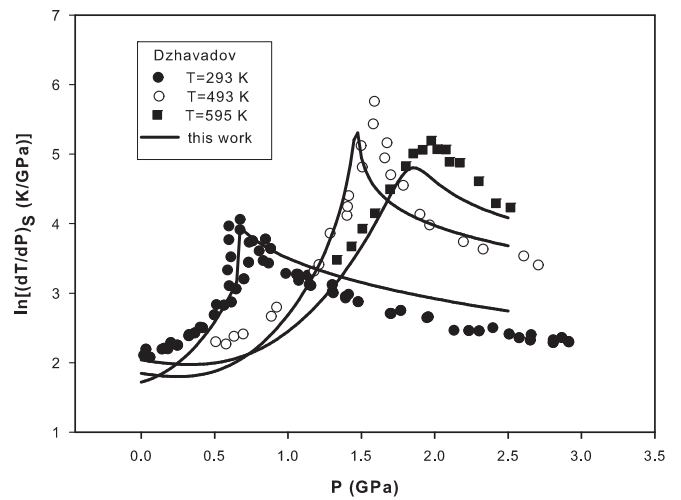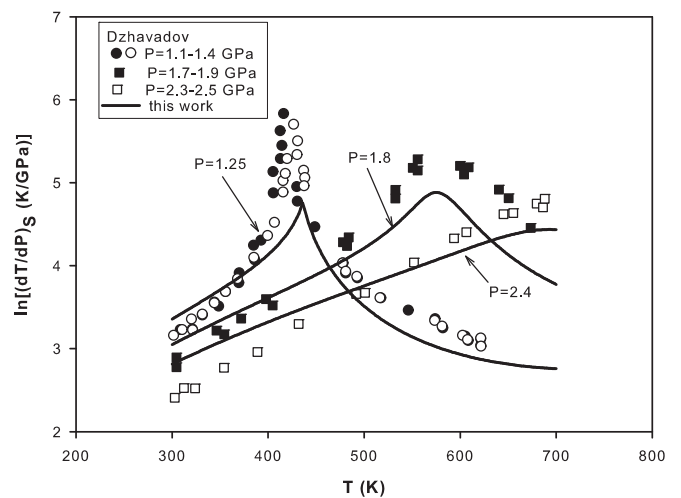

FIG. 6. $\ln(\partial T / \partial P)_S$ versus temperature (experimental data from Ref. 32).
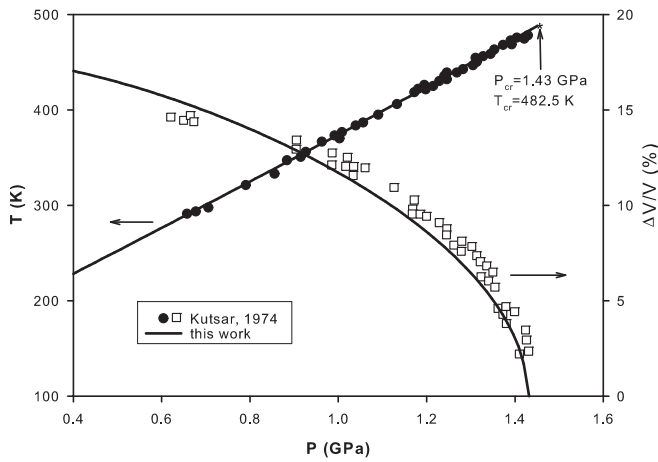
FIG. 7. Temperature and volume jump versus temperature for the γ-α phase transition on the phase equilibrium line (experimental data from Ref. 33).

FIG. 9. Cerium phase diagram (experimental data from Refs. 26, 36–39).

equilibrium, $T^{\gamma\alpha}$, ends at the critical point with coordinates $P = 1.43$ GPa, $T = 482.5$ K. The dashed continuation of the γ-α boundary corresponds to the locus of equal concentrations of γ and α phases ($c = 0.5$). The calculated melting curve T_{melt} agrees well with the experimental melting curve,[36,38] reproducing a minimum at $P_{min} = 3.45$ GPa, $T_{min} = 940$ K close to the experimental minimum $P_{min} = 3.3$ GPa, $T_{min} = 935$ K.[29] The AP-model treatment for the α and γ phases assists in replicating the melt curve reasonably well. It is noted that for pressures below ~2.6 GPa cerium melts from its δ phase (BCC)[36] which is also not considered.

Two possible regions for the existence of the ε phase were considered. The first option comes from the α-ε transition curve proposed by Zhao and Holzapfel[39] (the curve T_{Zhao} in Fig. 9). For pressures above 12 GPa cerium melts from the ε phase and the melting curve could be used to constrain the EOS parameters of the ε phase. This variant of the phase diagram would suggest that the Hugoniot in the (P,T) plane would cross the α-ε transition line. Shock experiments could possibly observe this transition. The EOS parameters for cerium using
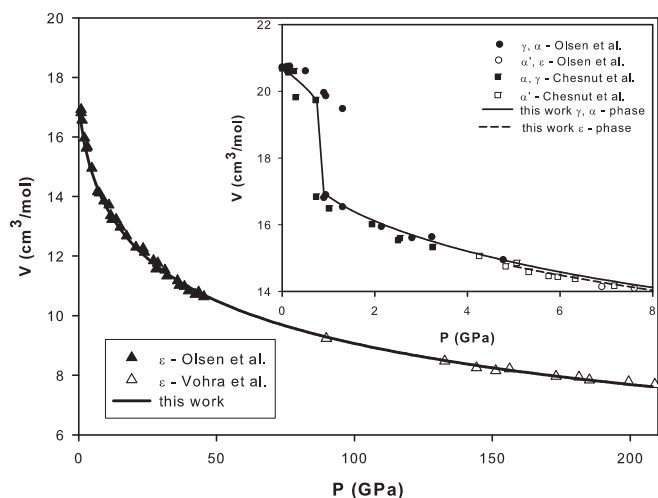

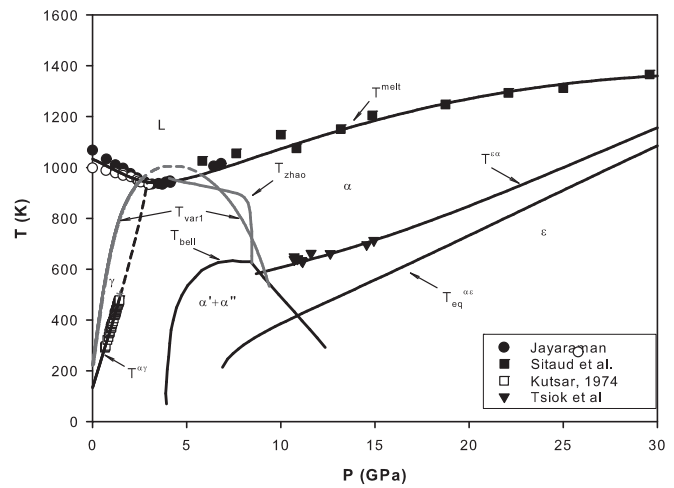FIG. 8. Isothermal compression to 208 GPa (experimental data from Ref. 25,34, and 35).

this assumption included the isothermal compression of ε cerium to 208 GPa,[25,34] a liquid cerium Hugoniot,[40–42] liquid cerium density and thermal expansion,[24] and the melting curve to 30 GPa.[38] The α-ε phase equilibrium line resulting from the equality of thermodynamic potentials between the α and ε phases is represented by the curve T_{var1} in Fig. 9. The curve is bell shaped and at pressures ~4–9 GPa is really shaped as stated in Zhao *et al.*[39] The comparison between the thermodynamic potentials of the α and ε phases showed the ε phase stability to be inside the bell. This result was unexpected because the EOS parameters for the ε phase were selected from experimental data at pressures beyond the bell, $P > 12$ GPa. Altering the EOS parameters in such a way to keep a reasonable agreement with experimental results only deformed the bell. Therefore, the assumption that the ε phase is adjacent to the liquid phase is contradictory; hence the α-ε transition curve proposed by Zhao[39] could be in error.

Another set of EOS parameters for the ε phase was produced using the electrical resistance experimental data.[26] In this study, samples were subjected to isobaric heating to ~600–700 K and pressures of 10–15 GPa, where they showed anomalies in the electrical resistance. The authors related this phenomena to the $\varepsilon \rightarrow \alpha$ phase transition.[26] In cooling the samples down to room temperature the reverse transformation was not observed which suggested a considerable temperature hysteresis for the transition. These experiments did not examine the crystalline structure that resulted from the transition, which is unfortunate. In this context, there remains some doubt whether the phase transition observed was actually the $\varepsilon \rightarrow \alpha$ transition.

Alternatively, we could propose that the transition observed by Tsiok[26] was some unknown phase X which is adjacent to both the liquid phase and the α phase. An EOS was constructed for this X phase and the X-α transition line, using the same experimental data as in the previous case, except it did not include the isothermal compression data for ε cerium. Also included was the additional condition that the X-α transition curve passes through the region of α' and α'' phases (i.e., crosses the dashed line T_{bell}). The results from this EOS parameter set showed that the X-α transition curve is bell

shaped too, similar to the aforementioned ε-α transition curve T_{var1}. A closer examination indicated that, again, the region inside the bell corresponded to the X phase and the melting curve is contiguous with the α phase. The initial assumption has led to a contradiction with calculation, thus suggesting that perhaps Tsiok *et al.*[26] were correct in assuming that the observed phase transition was the $\varepsilon \rightarrow \alpha$ transition.

Due to the above discussion, the EOS parameters presented in Table I are based on the data presented by Tsiok[26] and the isothermal compression data.[25,34,35] Figure 8 presents the compression curve for the ε phase for the higher pressure region plotted; the EOS parameters found in Table I predict this behavior with some certainty. Ideally, to better constrain the ε phase parameters, compression curves at temperatures above room temperature, as well as a more accurate location for the α-ε phase boundary than the existing literature would suggest, are needed.

It was assumed that the temperatures could be described by the equation $G_\alpha - G_\varepsilon + \Delta E_{\mathrm{hyst}} = 0$. Here ΔE_{hyst} is the energy needed to overcome the potential barrier at the beginning of the $\varepsilon \rightarrow \alpha$ transition and energy associated with its temperature hysteresis. Taking ΔE_{hyst} to be constant, the parameter E_{0K} for the ε phase is virtually redefined: $E_{0K} \rightarrow E_{0K} - E_{\mathrm{hyst}}$. After determining the EOS parameters which fit the experimental isothermal compression data up to 208 GPa (Fig. 8) and the $\varepsilon \rightarrow \alpha$ transition line (the curve $T^{\varepsilon\alpha}$ in Fig. 9), $(E_{0K} - E_{\mathrm{hyst}})/R = 44.5$ K is obtained. The estimated value of ΔE_{hyst} can be inferred by taking (based on some plausible grounds) the coordinates of a point on the ε-α equilibrium line. The midpoint of the region where the mixed α' and α'' phases exist at $T = 300$ K is the proposed point, which (at pressures from ~ 5 to ~ 12 GPa) separates the α and ε phases. The corresponding point of the ε-α equilibrium is thus taken to be at $T = 300$ K and $P = 8$ GPa. The required value of E_{0K} in the EOS for the ε phase is then $E_{0K}/R = 161.3$ K. Only this value is presented in Table I. The ε-α equilibrium line corresponding to this assumption is shown in Fig. 9 and is labeled as $T_{eq}^{\varepsilon\alpha}$. $\Delta E_{\mathrm{hyst}}/R$ is estimated to be $\approx 161.3 - 44.5 = 116.8$ K. This value is close to $E_{0K}/R = 161.3$ K which seems to cause the high-temperature hysteresis of the transformation. Note also that E_{0K}/R for the ε phase is lower than that for the γ_0 phase, and thus the ε phase should be represented with the AP model. However, the lack of experimental data precludes this.

IV. DYNAMIC EXPERIMENTAL DATA COMPARISON AND DISCUSSION

In considering the dynamic compression behavior of cerium, it has been shown[9,10] that the abnormal compressibility $[(\partial^2 V/\partial P^2)_S < 0]$ near the γ-α phase transition promotes the isentropic compression in cerium until the phase transition is complete. The model captures this behavior. Therefore the dynamic compression of cerium in the γ phase and the mixed γ and α phases is described by the equation $S(P,V) = S_{00}$, where S_{00} is entropy before the wave front. The shock compression behavior for the α and the liquid phases was calculated using the Rankine-Hugoniot equation $E - E_0 = \frac{1}{2}(P + P_0)(V_0 - V)$. The variables E, E_0, P, P_0, V, and V_0 represent energies, pressures, and specific volumes ($V = 1/\rho$)
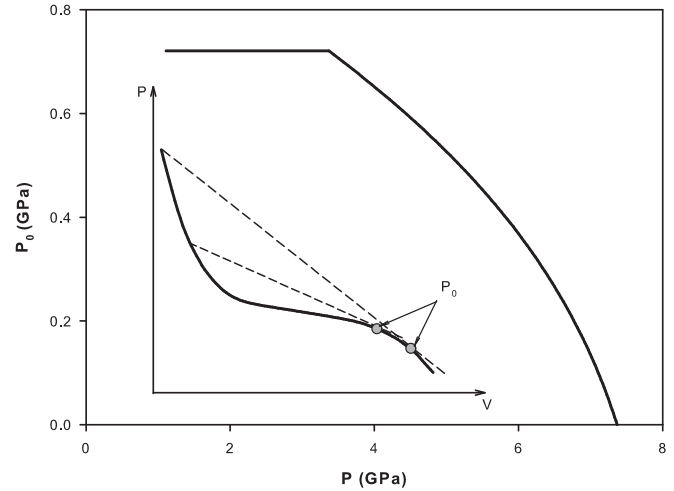

FIG. 10. The amplitude of the first (isentropic) wave versus pressure on the front of the second (shock) wave.

behind and ahead of the shock front. Energy, entropy, and specific volume for the mixed phase regions were calculated additively, specifically: $E = \xi E^i + (1 - \xi)E^j$, $S = \xi S^i + (1 - \xi)S^j$, $V = \xi V^i + (1 - \xi)V^j$, where ξ is concentration of particular phase i ($i,j = \gamma,\alpha,L$). The density of cerium at $T = 300$ K and $P = 0$ was $\rho_{00} = 6.74$ g/cm^3. The state ahead of the shock front at the end of the γ-α phase transition was determined by finding the point (V,P) where the tangency of the Rayleigh-Michelson line on the Hugoniot and the isentropic compression curve coincide:

$$\frac{P - P_0}{V - V_0} = \left[\frac{\partial P}{\partial V}(V_0)\right]_{S = S_{00}}. \qquad (8)$$

Figure 10 shows the phase precursor amplitudes P_0 ahead of the shock front as a function of the peak pressure observed behind the shock front. The inset in Fig. 10 graphically illustrates the solution for Eq. (8); the solid line represents the Hugoniot, and the dashed lines correspond to Rayleigh-Michelson lines. In this representation the effects of elasticity are ignored. For the amplitude of the phase transition wave, in the state before the shock front, the model predicts a constant phase transition stress up to 3.4 GPa, which then decreases until the shock overdrives the phase transition altogether at 7.4 GPa. This feature was discussed by Elkin *et al.*[9,10] and later experimentally confirmed by Borisenok *et al.*[13] The P_0 state shown in Fig. 10 is the pressure at which the γ-α phase transition begins. The prior work[9,10] showed the phase transition precursor disappearing at ~ 8.7 GPa. The principle difference comes from the modified EOS parameters for the γ_0 and α_0 phases.

In Fig. 11 the Hugoniot up to pressures of 30 GPa in the $(V/V_{00},P)$ plane is compared with the experimental data.[40–44] The sections marked with S^γ and $S^{\gamma\alpha}$ represent regions where isentropic compression occurs in the γ phase region and in the mixed $\gamma + \alpha$ phase regions. H^α, $H^{\alpha L}$, and H^L are the Hugoniots for the α phase, the mixed $\alpha + L$ phases, and the L phase (liquid), respectively. The vertical lines are included to show where the boundaries are along the principle Hugoniot. The agreement between calculated (equilibrium Hugoniot) and experimental results at low pressures after
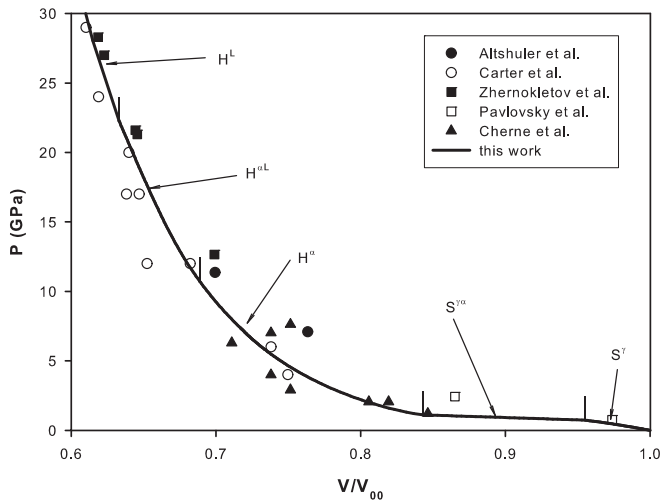
FIG. 11. Calculated Hugoniot up to 30 GPa in comparison with experimental data (Refs. [40–43]).

FIG. 12. Calculated Hugoniot over the entire range of experimentally studied pressures (Refs. [40–44]).

the completion of the γ-α phase transition suggests that the transition is kinetically fast. This most probably is a direct result of the electronic nature of the isomorphic γ-α phase transition. Considering that the low-pressure experimental Hugoniot data were not included in the fitting procedure, the agreement with the dynamic data suggests that the parameters chosen for the pure α and γ phase will provide a relatively accurate representation for using this equation of state in hydrodynamics calculations. Calculations suggest that a two-wave configuration will not occur at the cerium melt boundary.

We compare in Fig. 12 the calculated with the experimental Hugoniot up to 600 GPa. Up to ~160 GPa, the calculated Hugoniot agrees well with experiment. For pressures greater than 160 GPa (see inset in Fig. 12), the calculated pressures become much higher than the experimental data.[43,44] It is well understood that for these high compression ratios, the Vinet[17] cold curve begins to break down although our representation includes a higher order term. Up to 160 GPa, the simplified liquid model captures the compression behavior of liquid cerium. Perhaps a more realistic approach for the liquid state would be to allow the anharmonic-electronic Gruneisen parameter Γ_{AE} to vary with volume and temperature instead of letting it be a constant.

In Table III each of the pressure, volume, and temperature points along the room temperature dynamic compression curve of cerium is presented. The incipient melting values are in good agreement with the experimental numbers recently
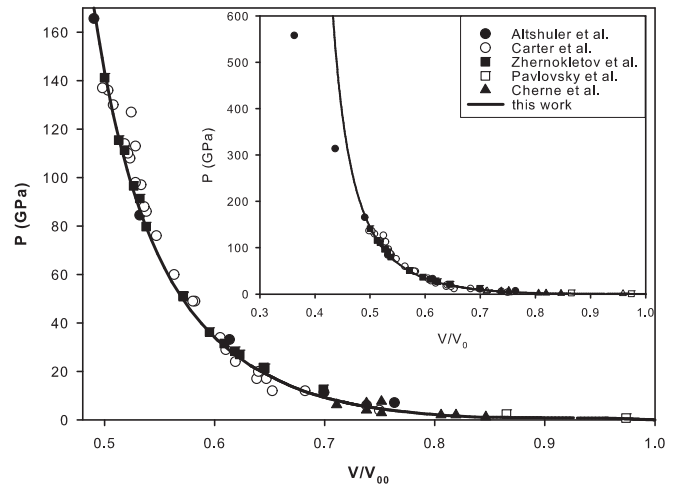
reported.[45,46] The $\gamma \rightarrow \alpha$ transition pressures are in good agreement with experimental data[43] as well. The completion of the melt transition at 22.3 GPa is greater than the 18 GPa reported by Jensen *et al.*[45] The completion of melt numbers are about 4 GPa greater than the experiment which could indicate that the liquid parameters or the liquid model may need some modification. The predicted Hugoniot shown in Figs. 11 and 12 for pressures greater than 22.3 GPa show a considerable amount of agreement. Although the liquid EOS was constructed from a combination of the Hugoniot data, the atmospheric pressure thermal expansion data, and the solid-liquid phase boundary, it is anticipated that the liquid EOS would predict accurately the isentropic release behavior or secondary shocks in the liquid region.

In Fig. 13 the experimental[42,46] and calculated sound velocities are shown for dynamic loading conditions. There is good agreement between the experimental and calculated sound velocities for pressures up to 160 GPa. The α-L mixed-phase region shows a smooth variation in sound speed with no significant jumps.

Calculated dynamic compression results and the calculated phase diagram in the (P,T) plane are shown in Fig. 14. The compression isentropes in the γ-phase region and the mixed $\gamma + \alpha$ phase region are indicated by S^γ and $S^{\gamma\alpha}$. The Hugoniots for the α, L, and $\alpha + L$ are given by H^α, H^L, and $H^{\alpha L}$, respectively. The marking scheme for the remaining marked curves is identical to those found in Fig. 9. From the Hugoniot calculations presented, it appears that

TABLE III. Characteristic pressure, volume, and temperature points on the room-temperature dynamic compression curve of cerium (isentrope and Hugoniot).

|	Pressure P (GPa)	Compression V/V_{00}	Temperature T (K)
Start of the γ-α transition on the compression isentrope	0.73	0.9546	308
End of the γ-α transition and beginning of shock compression in α phase	1.11	0.8429	401
Dissolution of the two-wave configuration (no phase precursor)	7.37	0.7169	849
Start of melting on the shock wave	10.74	0.6886	1091
End of melting on the shock wave	22.29	0.6329	1300
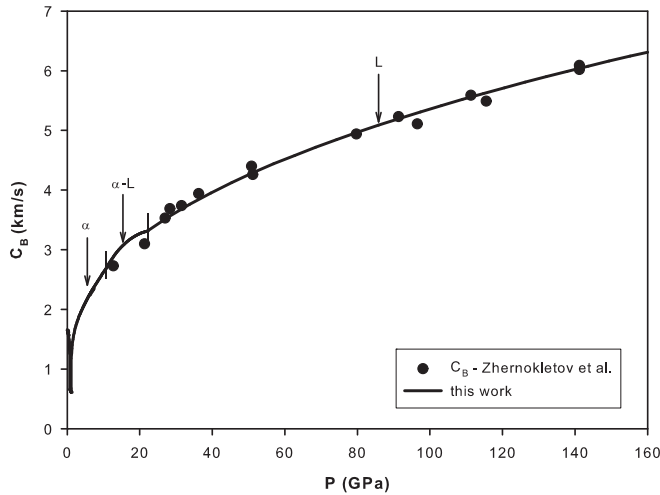
FIG. 13. Sound velocity on the shock front (experimental data from Refs. 42 and 46).

cerium melts from the α phase. The dashed lines represent the release isentropes from different shocked states, P_H. The lowest release isentrope ($P_H = 4$ GPa) begins in the α phase, then passes the region of the mixed $\alpha + \gamma$ phases near the critical point, and ends in the γ phase. The release isentropes $P_H = 8$ GPa and $P_H = 10$ GPa are above the critical point and indicate a smoother inflection through the extension of the α-γ boundary the farther they are away from the solid-solid critical point. The isentrope which begins on the mixed $\alpha + L$ phase line ($P_H = 16$ GPa) follows the α-L and departs from the boundary in the γ phase region. The highest calculated isentrope ($P_H = 30$ GPa) remains entirely in the liquid phase. It is clear from this diagram that the α-ε phase boundary should not be crossed dynamically from the principle Hugoniot. It may however be possible to cross the boundary via isentropic compression or double-shock experiments.

To better analyze experimental data or aid in the selection of loading parameters to study phase transitions under dynamic loading conditions, a useful piece of information to have would be the isentropic release paths with respect to the phase
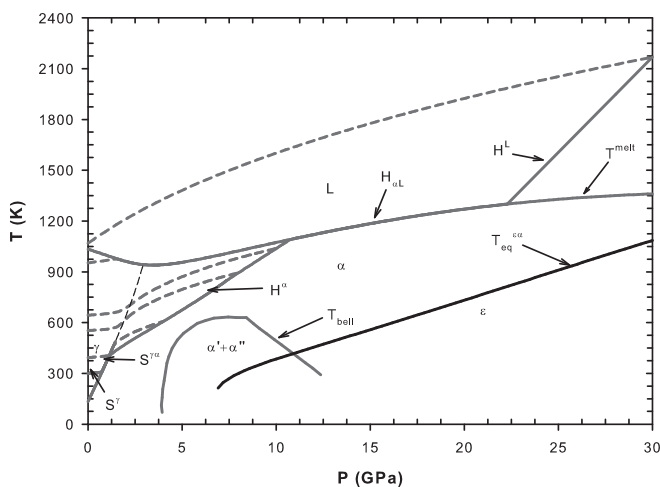

FIG. 14. Calculated Hugoniot, rarefaction isentropes, and phase diagram of cerium. The dashed lines show the rarefaction isentropes of cerium shocked to pressures $P_H = 4, 8, 10, 16, 30$ GPa.
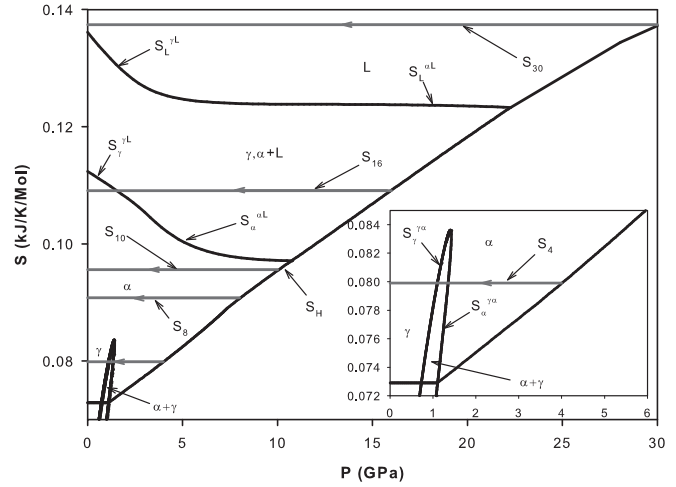

FIG. 15. (S, P) diagram for cerium. S_H is entropy on the Hugoniot; $S_i^{i\text{-}j}$ is entropy of phase i along i-j transformation line; $S_4, S_8, S_{10}, S_{16}, S_{30}$ are release isentropes from $P_H = 5, 8, 10, 16, 30$ GPa behind the shock front. The insert shows the region for small pressures.

diagram. To obtain this information, it is suggested that the rarefaction wave be determined with an (S, P) diagram, rather than a detailed isentrope projected on another plane. In Fig. 15, an (S, P) diagram of cerium is shown. The diagram presents entropy versus pressure on the Hugoniot, S_H, and the entropies of adjacent phases i and j on the i-j phase equilibrium curves, S_{ij}^i. For illustrative purposes the γ-α and α-L transitions are considered. The entropy at a specified pressure on the Hugoniot is determined from the curve $S_H(P)$. A line parallel to the abscissa is the isentrope. In the event that the isentrope crosses the curves $S_{ij}^i(P)$, the point formed by the intersection is the point where a phase transition occurs during the rarefaction process. As an illustration, Fig. 15 presents the isentropes which were shown in Fig. 14 in the (P, T) plane.

V. CONCLUSIONS

The proposed multiphase equation of state for cerium reproduces much of the available experimental data. Although the lower pressure dynamic experiments were not included in the fitting, the equation of state adequately predicts much of the Hugoniot data in the literature. The equation of state predicts the incipient melting pressures to within the experimental error. The concept of Aptekar-Ponyatovsky allowing for a binary mixture of electronic states, although yet to be verified, provides a thermodynamic framework to adequately capture the salient features of the $\alpha \rightarrow \gamma$ phase transition. The general lack of experimental data describing the thermophysical properties of the ε phase means that there is not much information on which to constrain the EOS parameters. Therefore experiments or *ab initio* calculations probing the thermophysical behavior of ε cerium are needed to provide a higher degree of credibility to the EOS for the ε phase. Thus the α-ε equilibrium curve should at this time be considered tentative.

We have outlined a multiphase thermodynamic framework which captures many of the properties of cerium. A high degree of certainty exists in this framework and thus should

be valid for high-fidelity numerical simulations requiring such a thermodynamically consistent model for the range where it has been shown to be valid.

APPENDIX A: SOLUTION TO GIBBS ENERGY FUNCTION

In order to find the extremum of the thermodynamic potential Eq. (4), it can be rewritten in dimensionless form by dividing everything through by RT. It is as follows:

$$g(c) = (1-c)g_{\alpha_0} + cg_{\gamma_0} + c(1-c)g_{\text{mix}}$$
$$+ c \ln c + (1-c)\ln(1-c), \quad \text{(A1)}$$

where g are the dimensionless Gibbs free energy of the respective phases or the mixing energy. Rearranging the equation and letting $\Delta g_{\alpha\gamma} = g_{\gamma_0} - g_{\alpha_0}$, the following is obtained:

$$g(c) = g_{\alpha_0} + c\Delta g_{\alpha\gamma} + c(1-c)g_{\text{mix}}$$
$$+ c \ln c + (1-c)\ln(1-c). \quad \text{(A2)}$$

Solving for the condition that defines the local extremum from Eq. (6) in terms of the unitless function above, the following is obtained:

$$g'(c) = \frac{\partial g}{\partial c} = \Delta g_{\alpha\gamma} + (1-2c)g_{\text{mix}} - \ln\frac{1-c}{c} = 0 \quad \text{(A3)}$$

and

$$g''(c) = -2g_{\text{mix}} + \frac{1}{c(1-c)} > 0. \quad \text{(A4)}$$

Solving the quadratic equation for c gives values at which $g'(c)$ exhibits an extremum. The two values for c are given by

$$c_1^* = \frac{1}{2}\left[1 - \sqrt{1 - \frac{2}{g_{\text{mix}}}}\right],$$
$$c_2^* = \frac{1}{2}\left[1 + \sqrt{1 + \frac{2}{g_{\text{mix}}}}\right]. \quad \text{(A5)}$$

Since $g'(0) = -\infty$, the c_1^* is a maxium and c_2^* is a minimum of $g'(c)$. Solutions of Eq. (A4) exist if $1 - \frac{2}{g_{\text{mix}}} > 0$ or $g_{\text{mix}} > 2$. For the conditions where $g_{\text{mix}} < 2$, the function does not have extremes; it is monotonic and hence, Eq. (A3) has only one solution. Figure 16 shows the behavior of $g'(c)$ at different g_{mix}. The condition $g_{\text{mix}} > 2$ is necessary but not sufficient for (A3) to have more than one solution. For Eq. (A3) to have three roots the following conditions must be met simultaneously:

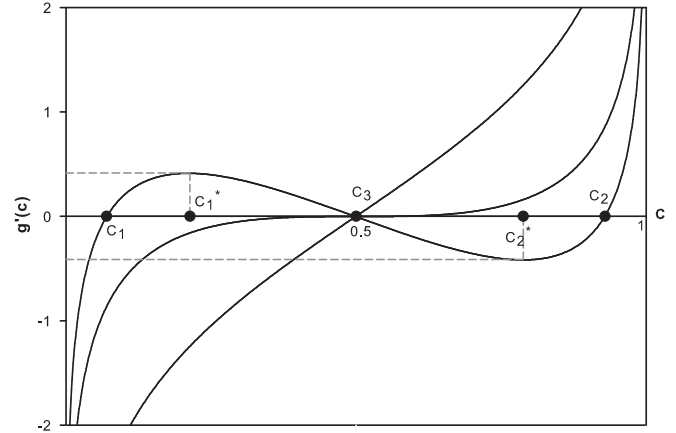$$g'(c_1^*) > 0 \quad \text{and} \quad g'(c_2^*) < 0. \quad \text{(A6)}$$

FIG. 16. Function $g' = g'(c)$ at different g_{mix}.

Combining Eqs. (A2), (A3), and (A4) with the requirement of Eq. (A6), for the states where $g_{\text{mix}} > 2$, it can be written as

$$\Delta g_{\alpha\gamma}^- = -g_{\text{mix}}\sqrt{1 - \frac{2}{g_{\text{mix}}}} + \ln\left(\frac{1 + \sqrt{1 - \frac{2}{g_{\text{mix}}}}}{1 - \sqrt{1 - \frac{2}{g_{\text{mix}}}}}\right),$$

$$\Delta g_{\alpha\gamma}^+ = g_{\text{mix}}\sqrt{1 - \frac{2}{g_{\text{mix}}}} - \ln\left(\frac{1 + \sqrt{1 - \frac{2}{g_{\text{mix}}}}}{1 - \sqrt{1 - \frac{2}{g_{\text{mix}}}}}\right), \quad \text{(A7)}$$

$$\Delta g_{\alpha\gamma}^- < \Delta g_{\alpha\gamma} < \Delta g_{\alpha\gamma}^+.$$

This equation defines the range of $\Delta g_{\alpha\gamma}$ where given the condition that $g_{\text{mix}} > 2$ there exist two local minima for the function $g(c)$. Let c_1 and c_2 ($c_1 < c_2$) be the concentrations corresponding to these minima in $g(c)$, and c_3 correspond to the concentration where the function $g(c)$ reaches a maximum. Based on this one could numerically find the roots of Eq. (A3) and the range for each root would be given by the following:

$$0 < c_1 < c_1^*,$$
$$c_2^* < c_2 < 1, \quad \text{(A8)}$$
$$c_1^* < c_3 < c_2^*.$$

In Fig. 17 the form of $g(c)$ is shown for different values of $\Delta g_{\alpha\gamma}$ as it crosses the boundaries defined by Eq. (A7).
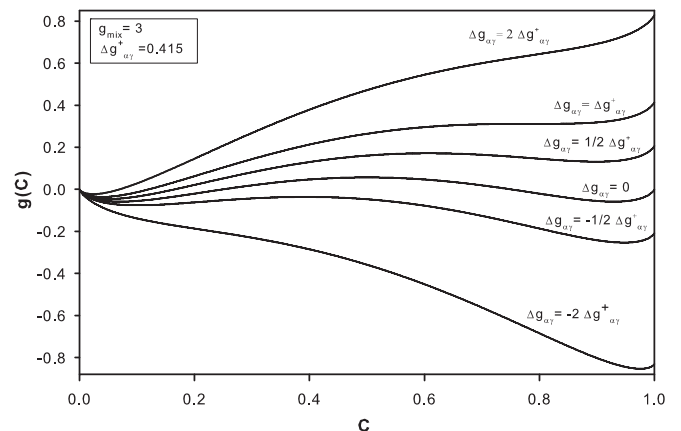

FIG. 17. Function $g = g(c)$ at different values of $\Delta g_{\alpha\gamma}$.

Considering the above equations, there are several possible regions as a function of the value that $\Delta g_{\alpha\gamma}$ takes. They are as follows:

(a) In the region where $\Delta g_{\alpha\gamma}$ is greater than the upper boundary of Eq. (A7), the function $g(c)$ has one minimum at $c < 1/2$. This region represents the region for α phase stability.

(b) In the region where $\Delta g_{\alpha\gamma}$ is positive yet below the upper boundary of Eq. (A7), the function $g(c)$ exhibits a second local minimum at $c > 1/2$. This implies that the γ phase is metastable and the α phase remains the equilibrium phase, due to the minimum being deeper.

(c) At $\Delta g_{\alpha\gamma} = 0$, both minima are identical in depth and symmetric about $c = 1/2$. Here both the γ and the α phases are in equilibrium.

(d) In the region where $\Delta g_{\alpha\gamma}$ is negative yet above the lower boundary of Eq. (A7), the second local minimum gets deeper than the first one. The γ phase is thermodynamically stable while the α phase is considered to be a metastable phase.

(e) When $\Delta g_{\alpha\gamma}$ is less than the lower boundary found in Eq. (A7), only one minimum of $g(c)$ is found at $c > 1/2$. The γ phase is the only stable phase present.

From the above, it can be inferred that when $g_{\mathrm{mix}} = 2$, Eq. (A3) has only one solution and thus, defines the solid-solid critical point on the phase equilibrium curve. Reintroducing the dimensional parameters, namely, RT, G_{mix} equals $2RT_{cr}$.

[1]D. J. Andrews, J. Phys. Chem. Solids **34**, 825 (1973).

[2]J. N. Johnson, D. B. Hayes, and J. R. Asay, J. Phys. Chem. Solids **35**, 501 (1974).

[3]D. B. Hayes, J. Appl. Phys. **46**, 3438 (1975).

[4]S. Pecker, S. Eliezer, D. Fisher, Z. Henis, and Z. Zinamon, J. Appl. Phys. **98**, 043516 (2005).

[5]A. A. Correa, L. X. Benedict, D. A. Young, E. Schwegler, and S. A. Bonev, Phys. Rev. B **78**, 024101 (2008).

[6]C. Mabire and P.-L. Hereil, J. Phys. IV (France) **10**, 749 (2000).

[7]C. Mabire and P.-L. Hereil, in *Shock Compression of Condensed Matter–1999*, AIP Conf. Proc. 505, edited by M. D. Furnish, L. C. Chhabildas, and R. S. Hixson (American Institute of Physics, New York, 2000), pp. 93–96.

[8]J. C. Boettger and D. C. Wallace, Phys. Rev. B **55**, 2840 (1997).

[9]V. M. Elkin, E. A. Kozlov, E. V. Kakshina, and Y. S. Moreva, Phys. Met. Metallogr. **101**, 208 (2006).

[10]V. M. Elkin, E. A. Kozlov, E. V. Kakshina, and Y. S. Moreva, in *Shock Compression of Condensed Matter–2005*, AIP Conf. Proc. 845, edited by M. D. Furnish, M. Elert, T. P. Russell, and C. T. White (American Institute of Physics, New York, 2006), pp. 77–80.

[11]I. L. Aptekar and E. G. Ponyatovsky, Fiz. Met. Metalloved. **25**, 777 (1968).

[12]I. L. Aptekar and E. G. Ponyatovsky, Fiz. Met. Metalloved. **25**, 1049 (1968).

[13]V. A. Borisenok, V. G. Simakov, V. A. Volgin, V. M. Bel'skii, and M. V. Zhernokletov, Combustion, Explosion, and Shock Waves **43**, 476 (2007).

[14]I.-K. Jeong, T. W. Darling, M. J. Graf, T. Proffen, R. H. Heffner, Y. Lee, T. Vogt, and J. D. Jorgensen, Phys. Rev. Lett. **92**, 105702 (2004).

[15]E. D. Chisolm, S. D. Crockett, and D. C. Wallace, Phys. Rev. B **68**, 104103 (2003).

[16]D. C. Wallace, Phys. Rev. B **46**, 5242 (1992).

[17]P. Vinet, J. H. Rose, J. Ferrante, and J. R. Smith, J. Phys. Condens. Matter **1**, 1941 (1989).

[18]A. Schiwek, F. Porsch, and W. B. Holzapfel, High Press. Res. **22**, 407 (2002).

[19]M. J. Lipp, D. Jackson, H. Cynn, C. Aracne, W. J. Evans, and A. K. McMahan, Phys. Rev. Lett. **101**, 165703 (2008).

[20]L. N. Dzhavadov, Phys. Solid State **47**, 2223 (2005).

[21]J. H. Holland, *Adaptation in Natural and Artificial Systems: An Introductory Analysis with Applications to Biology, Control, and Artificial Intelligence* (University of Michigan Press, Ann Arbor, MI, 1975).

[22]D. E. Goldberg, *Genetic Algorithms in Search, Optimization, and Machine Learning* (Addison-Wesley Pub. Company, Reading, MA, 1989).

[23]V. N. Mikhaylov, V. M. Elkin, and T. Y. Mikhaylova, Tech. Rep. Preprint 232, VNIITF, 2008.

[24]L. L. Besukladnikova, V. I. Kononenko, and V. V. Torokin, High Temp. **27**, 370 (1989).

[25]Y. K. Vohra, S. L. Beaver, J. Akella, C. A. Ruddle, and S. T. Weir, J. Appl. Phys. **85**, 2451 (1999).

[26]O. B. Tsiok and L. G. Khvostantsev, J. Exp. Theor. Phys. (Russia) **93**, 1245 (2001).

[27]F. F. Voronov, V. A. Goncharova, and O. V. Stalgorova, Zh. Eksp. Teor. Fiz. **76**, 1351 (1979).

[28]J. P. Bastide, C. Loriers-Susse, H. Massat, and B. Coqblin, High Temp. **10**, 427 (1978).

[29]A. R. Kutsar, Dokl. Akad. Nauk SSSR **245**, 1360 (1979).

[30]F. H. Spedding, J. J. Mckeown, and A. H. Daane, J. Phys. Chem. **64**, 289 (1960).

[31]F. Barson, S. Legvold, and F. H. Spedding, Phys. Rev. **105**, 418 (1957).

[32]L. N. Dzhavadov, High Temp. High Press. **21**, 401 (1989).

[33]A. R. Kutsar and O. S. Ivanov, in *Phase Structure, Phase Transitions, and State Diagrams of Metal Systems* (Nauka Publishers, Moscow, 1974), pp. 76–80.

[34]J. S. Olsen, L. Gerward, U. Benedict, and J. P. Itie, Physica B & C **133B**, 129 (1985).

[35]G. N. Chesnut, W. W. Anderson, and J. Casson, in *Shock Compression of Condensed Matter–2005*, AIP Conf. Proc. 845, edited by M. D. Furnish, M. Elert, T. P. Russell, and C. T. White (American Institute of Physics, New York, 2006), pp. 45–48.

[36]A. Jayaraman, Phys. Rev. **137**, A179 (1965).

[37]T. E. Antonova, I. T. Belash, and E. G. Ponyatovskii, Fiz. Met. Metalloved. **51**, 131 (1981).

[38]B. Sitaud, J. Pere, and T. Thevenin, in *High-Pressure Science and Technology–1993*, AIP Conf. Proc. 309, edited by S. C. Schmidt, J. W. Shaner, G. A. Samara, and M. Ross (American Institute of Physics, New York, 1994), pp. 245–247.

[39]Y. Zhao and W. B. Holzapfel, J. Alloys Compd. **246**, 216 (1997).

[40]L. V. Altshuler, A. A. Bakanova, and I. P. Dudoladov, Zh. Eksp. Teor. Fiz. (USSR) **53**, 1967 (1967).

[41]W. J. Carter, J. N. Fritz, S. P. Marsh, and R. G. McQueen, J. Phys. Chem. Solids **36**, 741 (1975).

[42]M. V. Zhernokletov, A. E. Kovalev, V. V. Komissarov, M. G. Novikov, M. A. Zocher, and F. J. Cherne, in *Shock Compression of Condensed Matter–2007*, AIP Conf. Proc. 955, edited by M. Elert, M. D. Furnish, R. Chau, N. C. Holmes, and J. Nguyen (American Institute of Physics, New York, 2007), pp. 117–120.

[43]M. N. Pavlovskii, V. V. Komissarov, and A. R. Kutsar, Combustion Explosion and Shock Waves **35**, 88 (1999).

[44]L. V. Altshuler, A. A. Bakanova, I. P. Dudoladov, E. A. Dynin, R. F. Trunin, and B. S. Chekin, J. Appl. Mech. Tech. Phys. **22**, 145 (1981).

[45]B. J. Jensen, F. J. Cherne, J. C. Cooley, M. V. Zhernokletov, and A. E. Kovalev, Phys. Rev. B **81**, 214109 (2010).

[46]M. V. Zhernokletov, A. E. Kovalev, V. V. Komissarov, M. G. Novikov, M. A. Zocher, and F. J. Cherne, J. Exp. Theor. Phys. **112**, 212 (2011).